Provided for non-commercial research and education use.
Not for reproduction, distribution or commercial use.

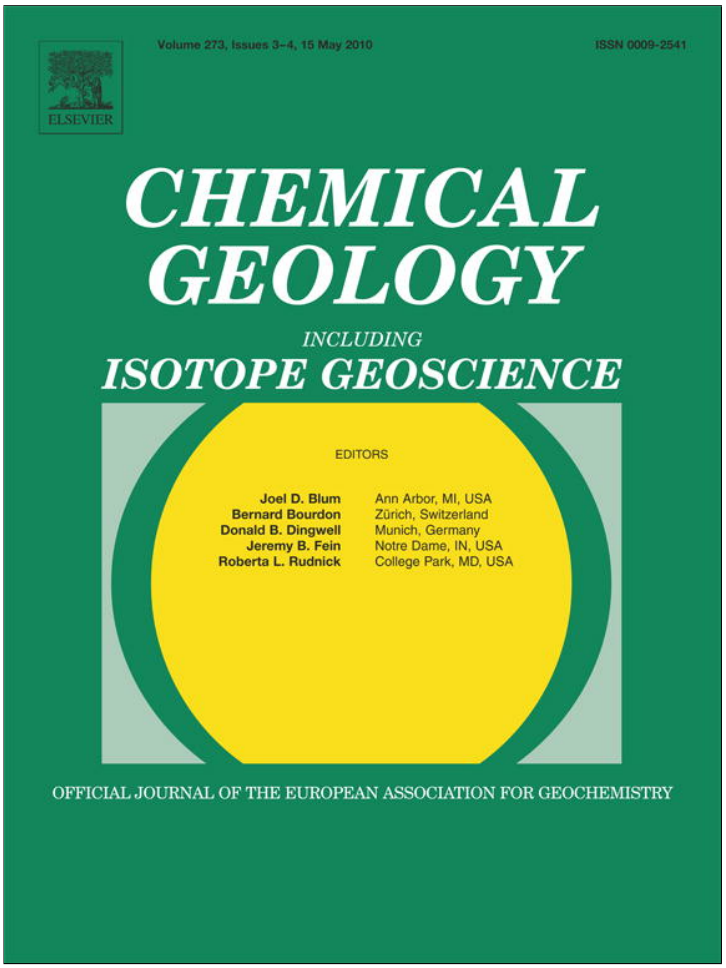

This article appeared in a journal published by Elsevier. The attached copy is furnished to the author for internal non-commercial research and education use, including for instruction at the authors institution and sharing with colleagues.

Other uses, including reproduction and distribution, or selling or licensing copies, or posting to personal, institutional or third party websites are prohibited.

In most cases authors are permitted to post their version of the article (e.g. in Word or Tex form) to their personal website or institutional repository. Authors requiring further information regarding Elsevier's archiving and manuscript policies are encouraged to visit:

http://www.elsevier.com/copyright

Author's personal copy

Chemical Geology 273 (2010) 300–313

Contents lists available at ScienceDirect

Chemical Geology

journal homepage: www.elsevier.com/locate/chemgeo

The effects of K-metasomatism in the Bahía Laura Volcanic Complex, Deseado Massif, Argentina: Petrologic and metallogenic consequences

G.N. Páez [a,b,*], R. Ruiz [a], D.M. Guido [a,b], S.M. Jovic [a,b], I.B. Schalamuk [a,b]

[a] Instituto de Recursos Minerales (INREMI), Universidad Nacional de La Plata, Calle 64 esquina Calle 120, (1900) La Plata, Provincia de Buenos Aires, Argentina
[b] Consejo Nacional de Investigaciones Científicas y Técnicas (CONICET), Buenos Aires, Argentina

ARTICLE INFO

Article history:
Received 1 September 2009
Received in revised form 12 March 2010
Accepted 15 March 2010

Editor: D.B. Dingwell

Keywords:
Deseado Massif
Epithermal
Metasomatism
Alteration
Volcanic glass

ABSTRACT

The Deseado Massif is a 60 000 km^2 geological region located in southern Argentinean Patagonia. The most important geological feature of this area is an extensive plateau characterized by complex and long-lived Middle to Upper Jurassic volcanism, composed of intermediate to acid volcanic rocks of the Bahía Laura Volcanic Complex. This voluminous volcanism originated in a widespread extensional environment that affected all of Patagonia, related to the opening of the Atlantic Ocean. The volcanic rocks are genetically related to Jurassic epithermal deposits. Consequently the region is an important gold and silver producer with four operational mines (Cerro Vanguardia, Mina Martha, Manantial Espejo and San José) and more than 50 epithermal occurrences undergoing different levels of exploration. Potassic metasomatism identified in the Bahía Laura Volcanic Complex is difficult to recognize in hand specimen, but is characterized by K_2O/Na_2O ratios higher than 2.5 and L.O.I. values lower than 3 wt.%, and affects only rocks with silica contents over 68 wt.%. The metasomatism produced an intense geochemical change in the affected rocks, with significant additions of K_2O, Rb, Au, Sb, W and a minor enrichment in Cs, Cu, As, and probably Ag and Hg. Strongly depleted elements are MgO, CaO, Na_2O, P_2O_5, MnO, Sr and U, whereas FeOt, TiO_2, L.O.I., Pb and Zn are moderately depleted. Finally, SiO_2, Al_2O_3, Mo and most trace elements and REE remained almost invariant during increasing metasomatism. Strong similarities in lithologies and geochemical signatures observed in K-metasomatized areas around the world, regardless of their geological settings and fluid origins, suggest that volcanic glass probably played an important role as an ion exchanger during alteration. Due to the high mobility of elements that occurs during K-metasomatism, no classification or discrimination diagram based on major elements, TiO_2 or Rb are considered to be valid for the chemical characterization of volcanic rocks based on metasomatized samples. The precious and base metals enrichment/depletion pattern of K-metasomatized rocks is identical to the geochemical signature observed in the upper parts of low sulfidation environments from the Deseado Massif. This geochemical signature, along with spatial relations observed between K-metasomatized rocks and epithermal manifestations, implies that hydrothermal fluids were responsible for the metasomatism observed in the Bahia Laura Volcanic Complex.

© 2010 Elsevier B.V. All rights reserved.

1. Introduction

The Deseado Massif is a 60 000 km^2 geological region located in the southern Argentinean Patagonia (Fig. 1). The most important geological feature of this area is an extensive plateau characterized by a complex and long-lived (more than 30 Ma) Middle to Upper Jurassic volcanic event, composed of intermediate to acid volcanic rocks of the Bahía Laura Volcanic Complex (Feruglio, 1949; Féraud et al., 1999; Riley et al., 2000). This voluminous volcanism originated during a widespread extensional event that affected all of Patagonia, related to the opening of the Atlantic Ocean (Pankhurst and Rapela, 1995).

The volcanic rocks are genetically related to Upper Jurassic epithermal deposits (Arribas et al., 1996; Schalamuk et al., 1997; Guido and Schalamuk, 2003; Echavarría et al., 2005; Fernandez et al., 2008). Consequently the region is an important gold and silver producer with four operational mines (Cerro Vanguardia, Mina Martha, Manantial Espejo and San José) and more than 50 epithermal occurrences undergoing different levels of exploration.

Lithogeochemical studies from several areas within this region show anomalously high values of K_2O along with extremely low values of Na_2O, indicating a secondary enrichment in potassium and leaching of sodium. K-metasomatism, an alteration characterized by the interaction of a K-rich fluid and the host rocks, has been proposed to explain these chemical changes (Sruoga, 1989; Guido, 2002; Echeveste, 2005).

This contribution examines the nature of the K-metasomatism affecting Jurassic volcanic rocks of the Deseado Massif and aims to define the origin and nature of the fluids that caused the alteration,

* Corresponding author. Instituto de Recursos Minerales (INREMI) Calle 64 esquina Calle 120, (1900) La Plata, Provincia de Buenos Aires, Argentina. Tel./fax: +54 221 4225648.
E-mail address: marduk_paez@yahoo.com.ar (G.N. Páez).

0009-2541/$ – see front matter © 2010 Elsevier B.V. All rights reserved.
doi:10.1016/j.chemgeo.2010.03.007

Author's personal copy

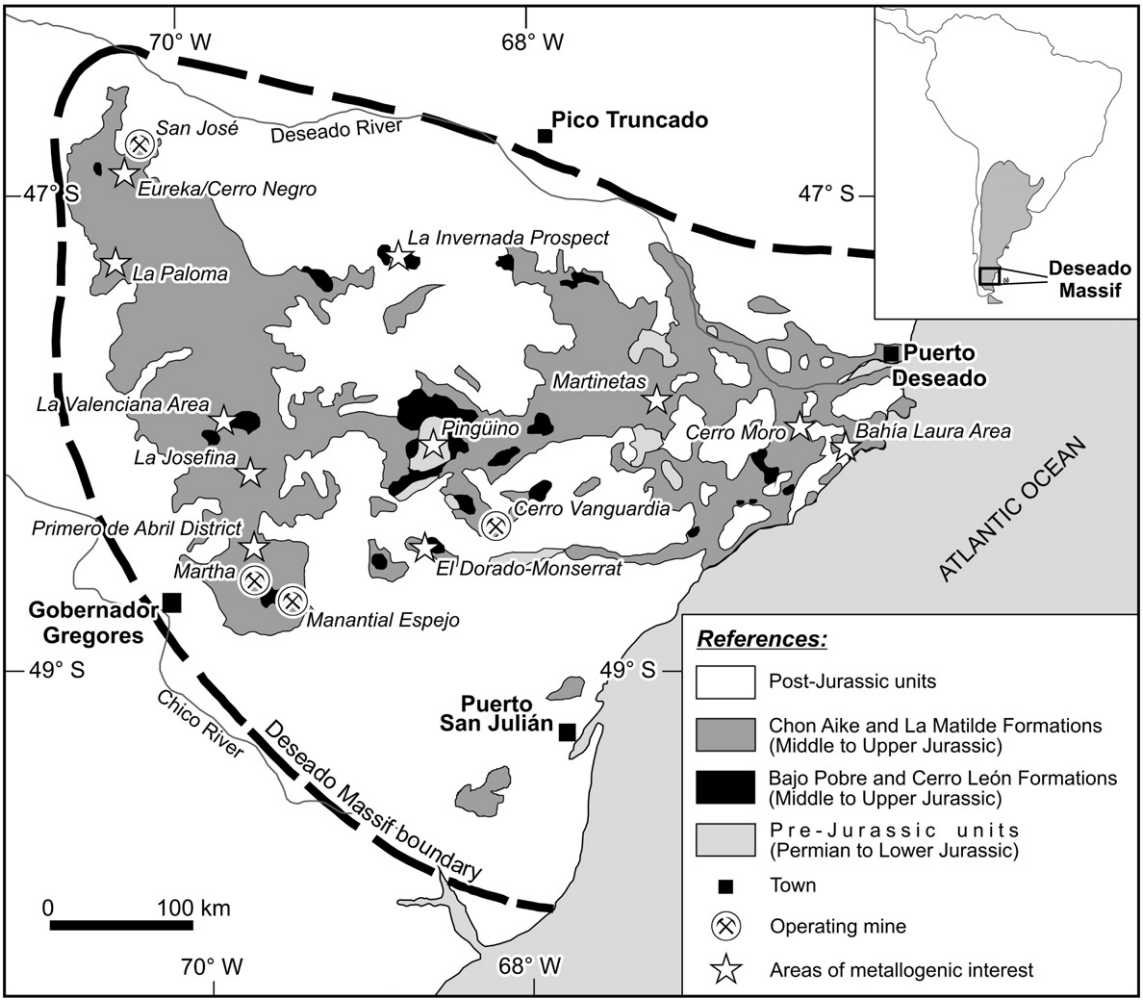

Fig. 1. Simplified geological map of the Deseado Massif showing the distribution of Jurassic volcanics and locations of mine sites and areas of metallogenic interest.

analyzing the petrologic and metallogenic consequences for the Jurassic rocks and epithermal deposit.

2. Geological setting

2.1. The Bahía Laura Volcanic Complex

During the Middle to Upper Jurassic, a volcanic mega-event occurred in Patagonia, giving rise to the Chon Aike Large Igneous Province (Pankhurst et al., 1998; Pankhurst et al., 2000). In the Deseado Massif (Fig. 1), this event is represented by a volcanic suite that was named the Bahía Laura Volcanic Complex (BLVC) by Feruglio (1949) and Guido (2004), and consists of the Bajo Pobre, Cerro León, Chon Aike and La Matilde formations. The Bajo Pobre Formation is characterized by intermediate to basic calcalkaline volcanic rocks, mostly andesitic in composition (Panza and Haller, 2002). These rocks are dominated by lavas, with subordinated ash flow tuffs and volcanic agglomerates. The Cerro León Formation is typified by subvolcanic intrusions (porphyries, laccolites, sills and dikes), which represent the feeder facies and intrusive equivalents of the Bajo Pobre Formation rocks (de Barrio et al., 1999; Jovic et al., 2008). These rocks are best represented in the lower section of BLVC. The Chon Aike Formation is dominated by rhyolites, with minor dacites and trachydacites, of calcalkaline, peraluminous and high potassium signature. These rocks built an extensive rhyolitic plateau, dominated by vast volumes of pyroclastic material erupted as high fluidity ash flow tuffs. Pyroclastic rocks predominate, and ignimbrites represent the 90% of the outcrops, with subordinate amounts of intercalated lavas (Pankhurst et al., 1998; Panza and Haller, 2002; Guido, 2004). Finally, La Matilde Formation is a homogeneous sequence of ash fall tuffs and reworked volcaniclastic sediments formed in low energy fluvial and lacustrine settings, with minor intercalations of ash flow and fall tuff deposits (de Barrio et al., 1999). The Chon Aike and La Matilde formations are dominant in the middle to upper of the BLVC sequence. Intricate stratigraphic relationships characterize the BLVC, with multiple fingerings of different facies (Echeveste et al., 2001; Guido et al., 2006; López, 2006; Ruiz et al., 2008).

There are two different interpretations of the relationships among magmas that define the Bahía Laura complex. Pankhurst and Rapela (1995) point out that Bajo Pobre and Chon Aike formations have an identical initial $^{87}Sr/^{86}Sr$ ratio and εNd_t, indicating a common origin from an isotopically homogeneous magma source. This idea is also supported by Pankhurst et al. (1998) for the entire Chon Aike Large Igneous Province, including the Deseado Massif BLVC. However, Busà et al. (2001; 2003) and Fantauzzi (2003) propose a different origin for the intermediate and acid magmas based on petrogenetic modelling and melt inclusion studies. They indicate that Chon Aike rhyolites cannot form by crystal fractionation from the Bajo Pobre intermediate rocks.

2.2. The Deseado metallogenic province

The BLVC is characterized by numerous gold and silver epithermal deposits, leading Schalamuk et al. (1999) to define the Deseado Massif as an Au–Ag metallogenic province. Most Au–Ag occurrences within

Author's personal copy

the Deseado Massif correspond to the low sulfidation (LS) style (Guido and Schalamuk, 2003; Echavarría et al., 2005; Fernandez et al., 2008), but in the last five years intermediate sulfidation and polymetallic deposits also have been reported for this metallogenic province (Gonzalez Guillot et al., 2004; Guido et al., 2005). These deposits are commonly hosted in the BLVC rocks, mainly in the Chon Aike Formation pyroclastics. There are also epithermal occurrences in older pre-BLVC rocks of sedimentary or metamorphic nature.

The typical mineralization style consist of veins, veinlets, vein stockworks and hydrothermal breccias, which are strongly controlled by Jurassic rift structures, showing dominant NW and WNW orientations, with minor participation of NE and E–W directions. Gangue minerals are mostly of the silica group, mainly quartz with minor chalcedony and opal, and accompanied in some places by calcite, adularia, barite, fluorite and zeolites. The quartz textures are commonly massive, brecciated, crustiform and colloform banding with comb, cockade and lattice bladed textures. Metalliferous minerals are scarce, representing commonly less than 10% in volume. They are mainly pyrite, native gold, electrum, argentite, native silver, Ag-sulfosalts, hematite, sphalerite, galena and chalcopyrite. The geochemical signatures from quartz veins agree with LS epithermal deposits, with anomalies in precious metals (Au–Ag) and occasional anomalous contents of As, Sb, Hg, Mo, Pb, Zn, Mn and minor Cu (Echeveste et al., 2001; Ruiz and Guido, 2006). Hydrothermal alteration is only restricted to the proximity of the veins and is represented by silicification, argillization (illite, smectite, kaolinite), sericitization and propylitization. The latter is better developed in the intermediate to basic lava flows. Associated with the epithermal veins, widespread silica and carbonate Jurassic hot spring deposits are present (Schalamuk et al., 1997).

According to Guido and Schalamuk (2003), Schalamuk et al. (2005) and Jovic (2009), the hydrothermal fluids responsible for the epithermal deposits of this region were neutral to alkaline $H2O + NaCl + KCl \pm CaCl_2 \pm FeCl_2$ solutions, with 0.18 to 8 wt% eq. NaCl salinities and homogenization temperatures ranging from ~100° to 320 ° C (for quartz and adularia). Fluid $\delta^{18}O$ values between −6.4 and +5‰ for quartz suggest an important participation of meteoric waters in the hydrothermal solutions, whereas fluid $\delta^{34}S_{CDT}$ values between −2.5 and +5‰ indicate a magmatic source for the sulfur. The Deseado Massif epithermal veins and hot spring deposits were formed during the Jurassic widespread extensional event, contemporaneous with the last stages of the BLVC event (Arribas et al., 1996; Schalamuk et al., 1997; Guido and Schalamuk, 2003; Echavarría et al., 2005).

3. K-metasomatism of the Bahía Laura Complex

In general, the compositional changes occurring during K-metasomatism depend on both the original rock composition and the nature and composition of the fluids involved in the process. Typical rock signatures include increased amounts of K_2O, Ba, and Rb and decreased amounts of MgO, Na_2O, CaO, MnO, Sr, Cu, Zn, and Pb (Brooks, 1988; Hollocher et al., 1994; Cooke et al., 1998; Ennis et al., 2000). During the last decade, several lithogeochemical studies, mainly focused on the relationship between epithermal deposits and volcanism, have been conducted to characterize the BLVC in mining project areas. In all these studies, the K-metasomatism was generally neglected.

Post- to syn-depositional alteration is commonly mentioned for the BLVC rocks (Gust et al., 1985; Sruoga, 1989; Pankhurst et al., 1998; Echeveste, 2005; Riley et al., 2000; Guido, 2002; Echavarría et al., 2005), mostly in close spatial association with epithermal occurrences. This regional scale alteration reportedly shows an intense K-enrichment and minor Si-enrichment, with also an important loss of Na. Such chemical mobility is explained as hydrothermal alteration (Sruoga, 1989; Echeveste, 2005; Echavarría et al., 2005) or low-grade metamorphism (Gust et al., 1985). As K-metasomatized rocks are very difficult to recognize in hand specimen, their particular geochemical behavior makes the K_2O/Na_2O ratio a useful indicator of the intensity of the metasomatism, and has been used by many researchers (Sruoga, 1989; Echeveste, 2005; Guido, 2002; Echavarría et al., 2005) in the past decade to identify the presence of metasomatized rocks in the Deseado area.

3.1. Geochemistry

To analyze the effects of the K-metasomatism in BLVC rocks, a database was compiled using 68 unpublished whole-rock geochemical assays along with 350 other previously published analyses (Table 1).

Previously unpublished samples were submitted to Acme Analytical Laboratories in Vancouver, Canada, and analyzed with the Group 4A (major element) + 4B (trace element) analytical packages (http://acmelab.com). The crushed samples were fused with Li metaborate/tetraborate and then subsequently dissolved by dilute nitric digestion prior to major element analysis by ICP-ES and trace-element analysis by ICP-MS or ICP-ES. In addition a separate split was digested in Aqua Regia and analyzed by ICP-MS to report the precious and base metals contents. Loss on ignition (LOI) is by weigh difference after ignition at 1000 °C. Table 2 provides a list of major and trace elements used in the study along with their analytical detection limits.

Table 1
Compiled geochemical database.

Area	Number of assays	Major and minor elements	Trace and REE elements	Metals	Routine	Laboratory	Reference
El Dorado–Monserrat	21	Full suite[a] except L.O.I.	Rb, Sr, Y, Zr, Nb, Ba, La, Ce, Nd	None	XRF	Padova University, Italy	Echavarria (1997)
Bahia Laura	48	Full suite[a]	Rb, Sr, Y, Zr, Nb, Ba, Ce, Nd, Hf, Th, U	None	XRF	Trieste University, Italy	Guido (2002)
Manantial Espejo Mine	72	Full suite[a] except L.O.I.	Rb, Sr, Y, Zr, Nb, Ba, La, Ce, Nd	None	XRF	Trieste University, Italy	Echeveste (2005)
La Josefina	55	Full suite[a]	Rb, Sr, Y, Zr, Nb, Ba, La, Ce, Nd, Th, U	Cu, Pb, Zn	XRF	Padova University, Italy	Moreira (2005)
Cerro Negro Project	26	Full suite[a]	Rb, Sr, Y, Zr, Nb, Ba, Ce, Nd, Th, U	None	XRF	Trieste University, Italy	Lopez (2006)
La Valenciana	72	Full suite[a]	None	None	XRF	Trieste University, Italy	Alperin et al. (2007)
La Invernada Prospect	10	Full suite[a]	Full suite[a]	Au, Ag, Cu, Pb, Zn, As, Sb, Hg	ICP-MS	Acme Labs, Canada	Permuy and Guido (2008)
Pingüino Project	46	Full suite[a]	Full suite[a]	Au, Ag, Cu, Pb, Zn, As, Sb, Hg	ICP-MS	Acme Labs, Canada	Jovic (2009)
Martha Mine	10	Full suite[a]	Full suite[a]	Au, Ag, Cu, Pb, Zn, As, Sb, Hg	ICP-MS	Acme Labs, Canada	Authors unpublished data
Primero de Abril	56	Full suite[a]	Full suite[a]	Au, Ag, Cu, Pb, Zn, As, Sb, Hg	ICP-MS	Acme Labs, Canada	Authors unpublished data

[a] See Table 2 for details.

Author's personal copy

Precision and accuracy of the analyses were monitored by: (1) analysis of internationally recognized geochemical reference standard rock powders (six standards per batch); (2) analysis of split duplicate samples (one duplicated every 35 analyzed samples), and; (3) analysis of Acme Labs internal standards (four standards per batch). QA/QC indicates an analytical error (1σ in relative percent) of measurements as follows: K_2O, TiO_2, MnO, SiO_2, Al_2O_3, CaO, Fe_2O_3, MgO, P_2O_5 and $Na_2O \leq 0{,}25\%$; Pr, Nd and La ≤ 1%; Eu, Gd, Dy, Tm, Y, Sr, Ho, Ba, Ce, Yb and Er ≤ 2,5%; Lu, W, Rb, Cs, Tb, Sm, U, Hf and Pb ≤ 5%; Zr, Th, Zn, Ag, Ta, Hg, Mo, As and Nb ≤ 7,5%; and Cu, Au and Sb ≤ 15%.

All samples considered in this study belong to known mineralized districts from the Deseado Massif, including samples from El Dorado–Monserrat District (Echavarría, 1997), the Bahía Laura Area (Guido, 2002), Manantial Espejo Mine (Echeveste, 2005), La Josefina District (Moreira, 2005), Cerro Negro Project (López, 2006), La Valenciana Prospect (Alperin et al., 2007), La Invernada Prospect (Permuy and Guido, 2008), Pingüino Project (Jovic, 2009), Martha Mine and the Primero de Abríl District (this study). As a first approach to analyze the compositional changes that occurred during K-metasomatism, variations in the contents of SiO_2, loss on ignition (L.O.I.) and K_2O/Na_2O ratio were studied for the different lithologies of the entire BLVC.

The considered 418 samples range in SiO_2 contents from 50.17 to 84.71 wt.%, in K_2O values between 0.08 and 11.46 wt.%, in Na_2O

Table 2
Summary of compositional data.

	DL	Unmetasomatized (G1)						K-metasomatized (G2)						Model compositional change [a]
		n	Min	Max	Median	Mean	St deviation	*n*	Min	Max	Median	Mean	St deviation	
Major elements (wt.%)														
SiO_2	0.01	100	68.60	81.45	72.28	72.43	3.09	94	68.08	84.68	75.03	75.01	3.25	3.81
Al_2O_3	0.01	100	8.99	17.65	14.33	14.27	1.59	94	8.38	20.49	13.76	14.08	2.62	−3.94
FeOt	0.01	100	0.70	4.84	1.87	2.06	0.93	94	0.27	6.92	1.24	1.33	0.89	−33.70
MgO	0.01	100	0.03	2.13	0.41	0.51	0.43	94	0.01	1.17	0.17	0.24	0.21	−58.54
CaO	0.01	100	0.05	3.42	0.91	1.23	0.90	94	0.01	3.43	0.15	0.28	0.48	−83.46
Na_2o	0.01	100	1.73	8.12	3.00	3.03	0.70	94	0.06	2.41	0.63	0.72	0.55	−78.96
K_2O	0.01	100	0.09	6.28	4.67	4.53	0.80	94	2.25	11.46	7.23	7.31	1.87	54.98
TiO_2	0.01	100	0.04	0.68	0.19	0.22	0.13	94	0.03	0.61	0.11	0.15	0.11	−40.54
P_2o_5	0.001	100	0.01	0.36	0.04	0.06	0.05	94	0.01	0.16	0.02	0.03	0.03	−50.00
MnO	0.01	100	0.01	0.11	0.03	0.04	0.02	94	0.01	0.07	0.01	0.01	0.01	−66.67
LOI		85	0.74	2.90	1.96	1.90	0.60	51	0.20	2.75	1.50	1.57	0.70	−23.47
Total			97.32	100.36	99.92	99.79	0.42		97.43	100.87	99.92	99.88	0.33	
K_2O/Na_2O		100	0.01	2.42	1.56	158.00	0.35	94	2.51	112.63	13.06	20.52	18.69	739.58
Trace elements (ppm)														
Rb	0.1	73	5.00	291.00	172.00	174.96	47.33	94	70.00	1552.00	290.50	303.76	162.49	68.90
Sr	0.5	75	7.00	480.00	131.20	139.44	84.78	94	8.00	271.00	41.50	55.81	48.77	−68.37
Y	0.1	75	5.00	179.00	24.90	29.17	21.28	94	7.30	183.00	27.00	28.65	18.67	8.43
Zr	0.1	75	66.00	308.00	150.00	153.71	47.19	94	27.00	1123.00	122.00	136.24	166.78	−18.67
Nb	0.1	73	6.00	24.00	9.40	9.95	2.88	94	3.00	85.00	9.00	9.60	8.31	−4.26
Cs	0.1	19	1.60	40.40	5.40	8.07	8.68	29	1.20	24.00	7.90	8.07	4.72	46.30
Ba	1	71	34.00	3319.00	915.00	924.54	486.39	86	16.00	5045.00	960.00	1056.70	632.89	4.92
La	0.1	50	16.00	92.50	31.65	33.00	12.46	84	6.20	53.00	31.40	30.81	9.85	−0.79
Ce	0.1	73	0.00	175.70	64.00	69.15	30.43	94	10.10	141.00	58.00	56.63	18.94	−9.38
Pr	0.02	19	4.50	22.48	7.20	8.24	3.90	29	1.88	12.31	7.14	6.73	2.44	−0.83
Nd	0.3	73	0.00	78.30	27.60	29.30	13.84	93	6.20	55.00	25.00	25.82	9.04	−9.42
Sm	0.05	19	2.42	11.47	4.66	5.39	2.10	29	1.31	9.12	4.82	4.74	1.75	3.43
Eu	0.02	19	0.52	1.74	0.80	0.88	0.31	29	0.11	1.73	0.64	0.71	0.36	−20.00
Gd	0.05	19	1.49	8.42	4.13	4.51	1.78	29	1.27	7.30	4.33	3.98	1.52	4.84
Tb	0.01	19	0.30	1.13	0.72	0.74	0.25	29	0.21	1.23	0.72	0.67	0.23	0.00
Dy	0.05	19	1.81	5.80	4.16	4.13	1.26	29	1.18	6.55	3.86	3.75	1.23	−7.21
Ho	0.02	19	0.40	1.25	0.88	0.86	0.25	29	0.23	1.35	0.79	0.79	0.24	−10.23
Er	0.03	19	1.03	3.41	2.51	2.37	0.70	29	0.79	3.80	2.29	2.25	0.70	−8.76
Tm	0.01	19	0.19	0.56	0.40	0.39	0.11	29	0.16	0.62	0.39	0.38	0.11	−2.50
Yb	0.05	19	1.22	3.26	2.60	2.41	0.65	29	1.09	3.77	2.33	2.37	0.63	−10.38
Hf	0.1	19	2.40	5.90	4.30	4.22	1.06	29	2.80	5.50	3.90	3.92	0.62	−9.30
Lu	0.01	19	0.21	0.52	0.40	0.38	0.09	29	0.17	0.59	0.37	0.38	0.10	−7.50
Ta	0.1	19	0.30	1.00	0.80	0.72	0.20	29	0.40	1.40	0.90	0.85	0.27	12.50
Th	0.02	46	6.00	37.00	16.95	18.14	6.33	40	9.50	28.00	16.45	16.31	3.70	−2.95
U	0.1	45	1.30	10.00	4.60	4.55	2.14	40	1.70	9.00	2.90	4.00	2.17	−36.96
Metals[b]														
Ag	0.1	19	0.10	0.20	0.10	0.11	0.02	29	0.10	0.60	0.10	0.14	0.15	0.00
Au	0.5	19	0.50	2.60	0.50	0.88	0.57	29	0.50	3.90	1.00	1.27	0.91	100.00
Cu	0.1	23	1.00	67.00	4.00	7.05	13.32	30	1.00	39.40	4.65	7.04	6.99	16.25
Pb	0.1	23	0.70	35.00	13.00	13.24	7.32	30	2.80	305.70	9.80	28.84	55.72	−24.62
Zn	1	23	9.00	168.00	34.00	44.43	34.78	30	2.00	1454.00	20.00	98.65	273.59	−41.18
As	0.5	19	0.50	21.90	3.60	5.58	5.17	29	1.00	18.60	3.90	4.18	4.36	8.33
Hg	0.01	19	0.01	0.12	0.01	0.02	0.03	29	0.01	0.17	0.01	0.03	0.04	0.00
Sb	0.1	19	0.10	0.60	0.20	0.26	0.19	29	0.10	3.00	0.40	0.68	0.74	100.00
W	0.5	19	1.00	4.70	1.70	2.18	1.14	29	0.50	11.70	3.50	4.16	2.87	105.88
Mo	0.1	19	0.20	1.70	0.40	0.61	0.49	29	0.20	1.70	0.40	0.57	0.43	0.00

n = number of assays; DL = detection limit.
[a] Percent difference between unmetasomatized and metasomatized median compositions.
[b] All metal concentrations are in ppm, except for Au that is in ppb.

Author's personal copy

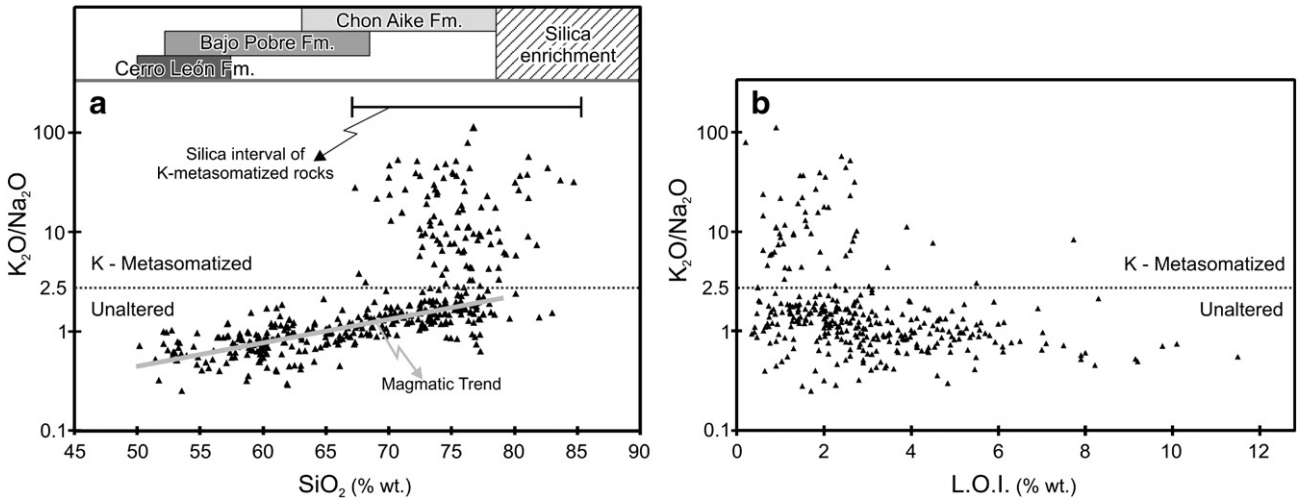

Fig. 2. Plot of K_2O/Na_2O ratio compared to a) SiO_2 ($n=418$) and b) L.O.I. values ($n=352$) for the entire Bahía Laura Complex silica interval.

contents from 0.06 to 8.12 wt.%, and in L.O.I. values between 0.2 and 11.5 wt.%. Moreover, the calculated K_2O/Na_2O ratio, also used as an indicator of the intensity of potassic metasomatism (Brooks, 1988; Sruoga, 1989; Hollocher et al., 1994 and Guido, 2002), shows a great variability, with values ranging from 0.01 to up to 112.63.

When the K_2O/Na_2O ratio is plotted with SiO_2 (Fig. 2a), two different populations are evident. The first shows a very good correlation and comprises K_2O/Na_2O values lower than 2.5 and silica contents between 50 and 77 wt.%. This pattern is interpreted as a magmatic differentiation trend. The second data population has >2.5 K_2O/Na_2O values and >68 wt.% SiO_2, and are interpreted as the K-metasomatized rocks. When samples are compared with respect to K_2O/Na_2O and L.O.I. values (Fig. 2b), those with ratios higher than 2.5 are characterized by a random array of low L.O.I. values, most of them between 1 and 3 wt.%. By contrast, samples with ratios lower than 2.5 show a good correlation, with a progressive decrease of K_2O/Na_2O with increasing L.O.I, indicating leaching of alkalis associated with a non K-metasomatic alteration.

As the only K-metasomatized rocks of BLVC are those with silica contents higher than 68% (dacitic to rhyolitic ash flow tuffs and lavas), the samples with lower values will not be considered herein, in order to show clear relationships. The resulting 194 samples (>68 wt.% SiO_2) were divided into two groups (G1 and G2) according to their K_2O/Na_2O ratios. Samples with ratios <2.5 were treated as fresh rocks (G1) and samples with >2.5 ratios were considered to be K-metasomatized (G2). This difference is also apparent when comparing K_2O vs. Na_2O contents (Fig. 3); in this case the same 2.5 K_2O/Na_2O value can be used to separate K-metasomatized from unaltered samples.

Table 2 summarizes the compositional data of G1 and G2 groups with minimum, maximum, median, mean and standard deviation values. As the compiled data are derived from different sources, the number of assays (n) considered for each element is detailed. Compositional values below the detection limit were matched to the detection limit of each dataset.

3.1.1. Major and minor element concentrations

Fig. 4 shows the behavior of major and some minor elements during increasing K-metasomatism in the Deseado Massif, using the K_2O/Na_2O ratio as an alteration intensity index. The altered and unaltered rocks were separated by the 2.5 K_2O/Na_2O ratio line. On each plot, the dispersion of the samples along the y-axis represents the natural

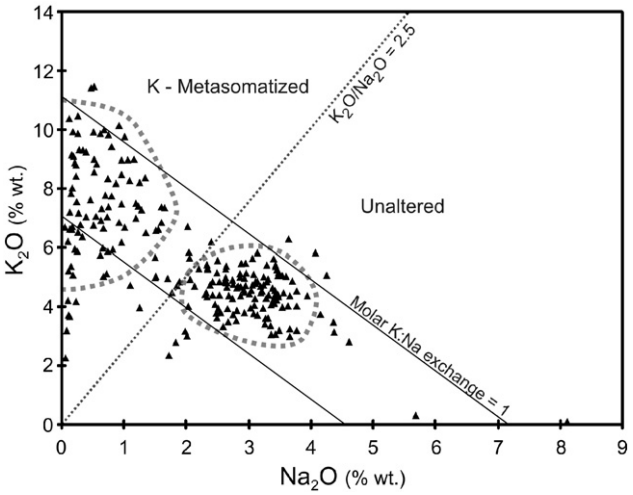

Fig. 3. Plot of K_2O vs. Na_2O for all Bahía Laura Complex samples above 68 wt.% SiO_2 ($n=194$). Two 1:1 molar K:Na exchange ratio lines are shown for comparison.

variability of the rock series due to magmatic differentiation over the silica range considered in this study (from 68 to 85 wt.%). As can be seen in Fig. 4 and Table 2, the metasomatism not only affected the contents of the different elements but also their variability.

SiO_2 and Al_2O_3 contents remain almost invariant during increasing metasomatism (Fig. 4a and b); however, silica shows a slight increase and aluminum shows a small decrease. In both cases a small increase in the variability can be observed. FeOt and MgO show a decrease in content and a small decrease in variability (Fig. 4c and d). The CaO concentrations and their variability become progressively less with increasing metasomatism (Fig. 4e). Na_2O and K_2O showed the opposite behavior during K-metasomatism (Fig. 4f and g). The potassium content increased as the sodium content became progressively less. In both cases the variability increases toward the most intensely metasomatized rocks. Finally, minor elements, represented by TiO_2, MnO and P_2O_5, show a similar behavior, with decreasing concentrations and almost no change in variability. However, TiO_2 concentration shows a particular behavior with an intense decrease with low intensity K-metasomatism and then a progressive increase with high K_2O/Na_2O ratios (Fig. 4h).

Fig. 4. Plots comparing the K_2O/Na_2O ratio with major and minor elements. The grey circles and diamonds represent the median compositions of unaltered and metasomatized samples, respectively, as expressed in Table 2. All plotted samples have SiO_2 contents above 68 wt.% ($n=194$).

Author's personal copy

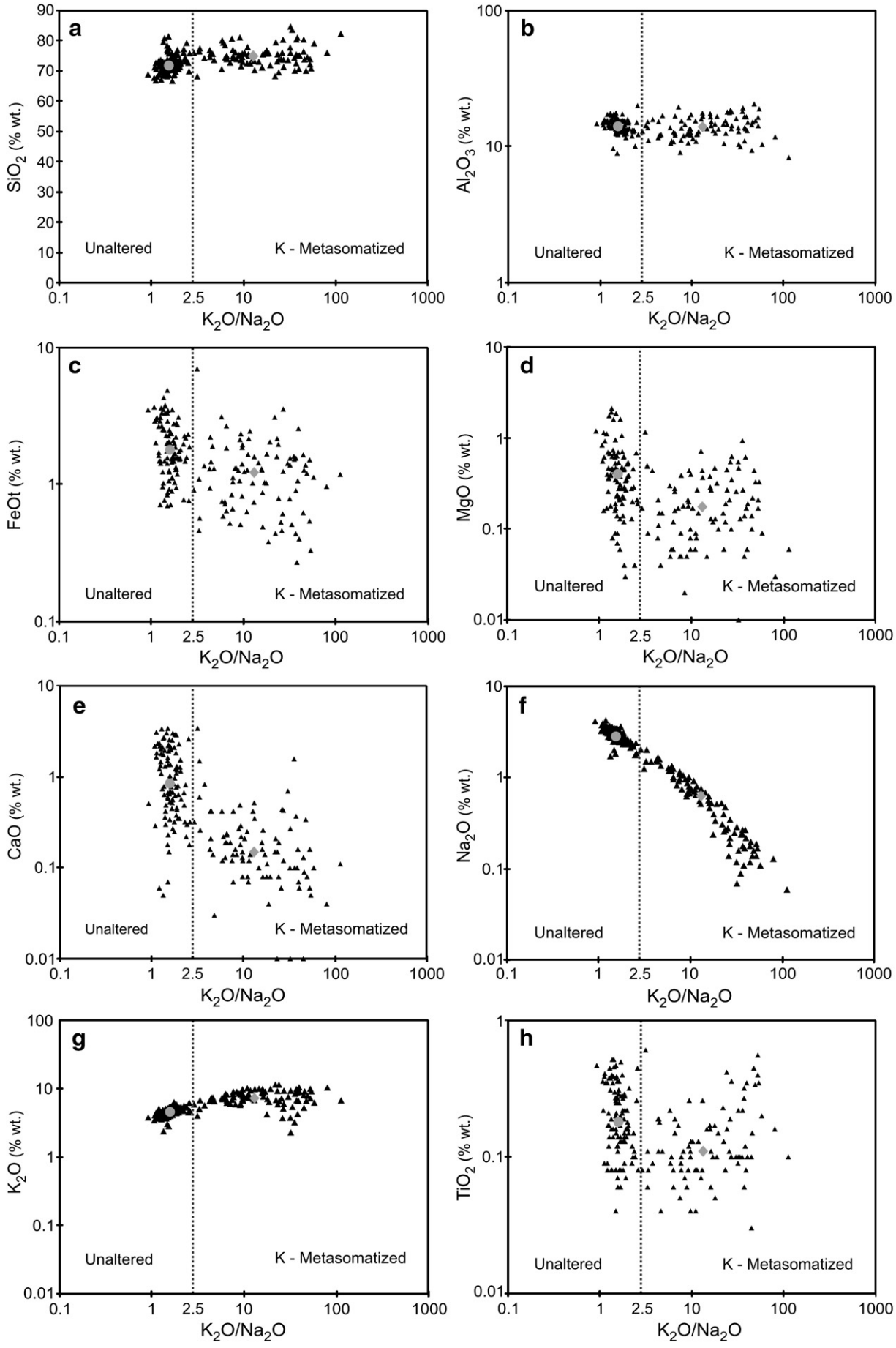

Author's personal copy

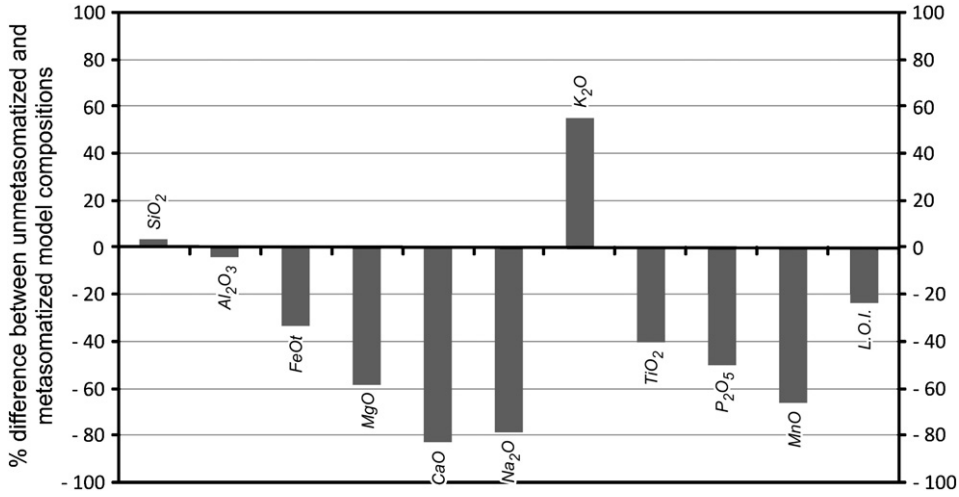

Fig. 5. Enrichment/depletion diagram for major and minor elements summarizing the compositional changes occurred during K-metasomatism. The percent compositional change is based on median values of unaltered compared to metasomatized samples as expressed in Table 2; positive values indicate enrichment in K-metasomatized rocks, while negative values indicate leaching.

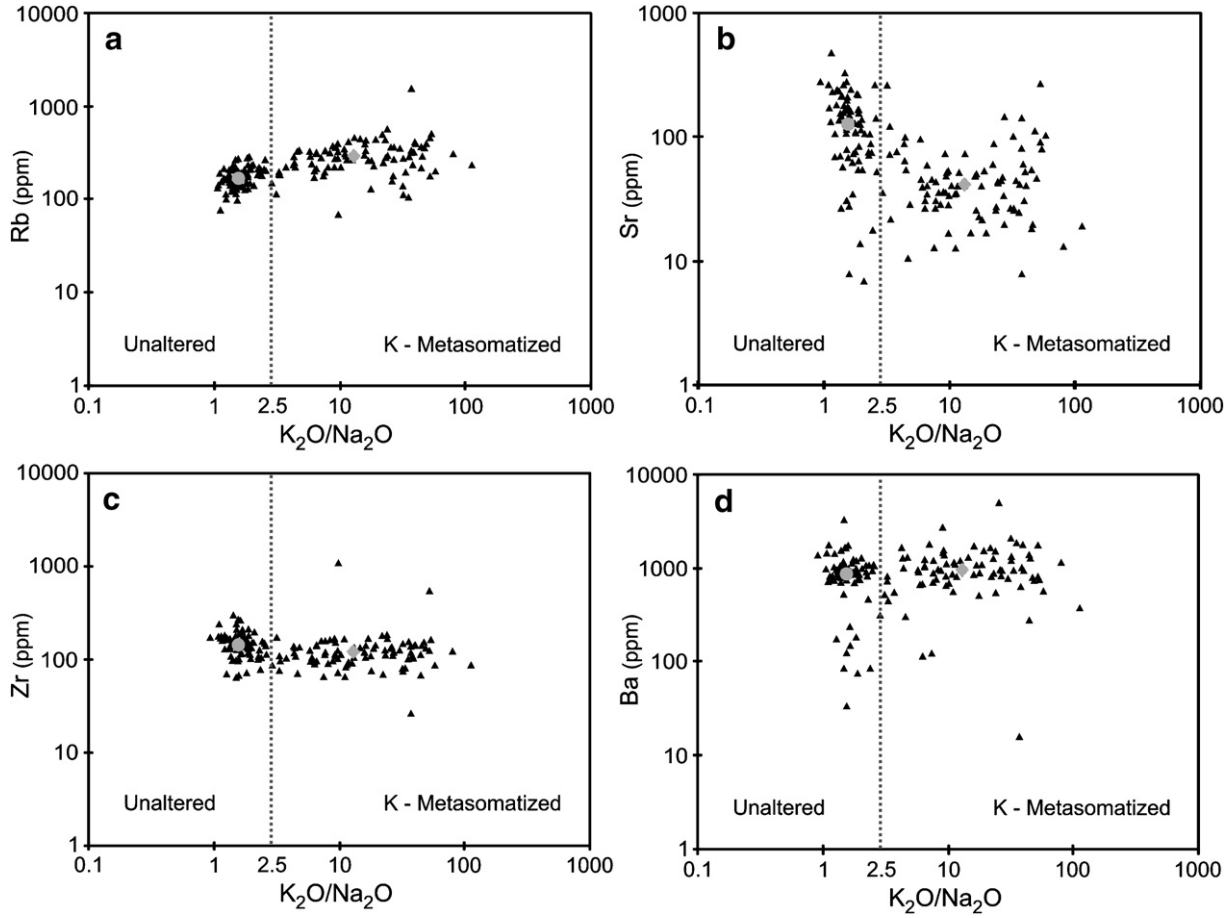

Fig. 6. Plots between K_2O/Na_2O ratio and a) Rb ($n=167$); b) Sr ($n=169$); c) Zr ($n=169$); d) Ba ($n=157$). The grey circles and diamonds represent the median compositions of unaltered and metasomatized samples, respectively, as expressed in Table 2. All plotted samples have SiO_2 contents above 68 wt.%.

Model compositions were constructed using median compositional values to estimate the net compositional change occurring during K-metasomatism (Table 2). The median value was preferred over the mean in order to reduce the impact of outliers on the considered datasets. The model compositional changes (MCC) in element concentrations were calculated with respect to G1 using the expression: $MCC=[(E_{G1}-E_{G2})/E_{G1}]*100$, in which E_{G1} is the element median concentration in G1 (unaltered group) and E_{G2} is the element median concentration in G2 (metasomatized group). Elements with positive MCC values increased their concentration during K-metasomatism, whereas negative values decreased the concentration (Table 2). Note that the variance of some elements in both groups is large, mostly due

Author's personal copy

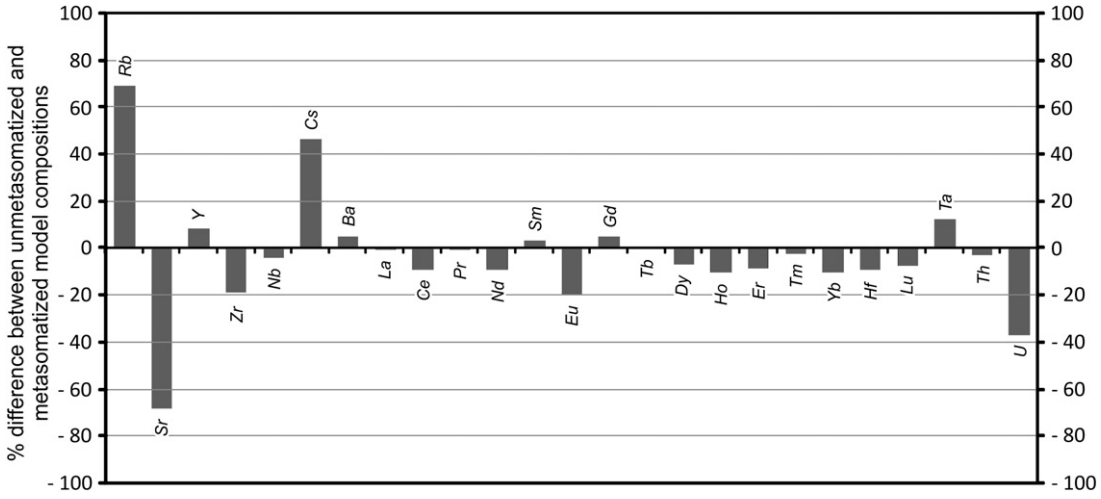

Fig. 7. Enrichment/depletion diagram for trace and rare earth elements summarizing the compositional changes occurred during K-metasomatism. The percent compositional change is based on median values of unaltered compared to metasomatized samples as expressed in Table 2; positive values indicate enrichment in K-metasomatized rocks, while negative values indicate leaching.

to the inherited igneous variability. While model compositions must be used with caution, a comparison of median values of each element with bulk compositional data (big grey symbols in Fig. 4) suggests a good correlation between the median model compositions and the behavior of each element during increasing K-metasomatism. An enrichment/depletion diagram using the MCC values from BLVC (Fig. 5) indicates that K_2O is strongly enriched in the K-metasomatized rocks, with an enrichment factor of about 54.98%. SiO_2 and Al_2O_3 remain almost immobile, and FeOt, TiO2 and L.O.I. are depleted between −23% and −33%. Finally MgO, CaO, Na_2O, P_2O_5 and MnO show a strong depletion in the metasomatized rocks, reaching MCC values lower than −50%.

3.1.2. Trace element and REE concentrations

The behavior of trace elements during increasing K-metasomatism in the Deseado Massif is illustrated in Fig. 6 for Rb, Sr, Zr and Ba, using the K_2O/Na_2O ratio as an alteration intensity index. In particular, the trace elements can be divided into three groups based on their variations during increasing metasomatism (Table 2). Rb and Cs show an increase in concentrations; Sr and U decrease significatively. Furthermore, Y, Zr, Nb, Zr, Hf, Ta and Th remain almost invariable, showing either a small increase or decrease. The variability of Sr, Y, Ce and Hf are characterized by small decreases; whereas, Sr, Zr, Nb, and Ba increase their variability due to metasomatism. Finally Ta and U show no change in variability. Because of the opposite behavior of Rb and Sr (Fig. 6a and b), the Rb/Sr ratio is also useful to identify the presence of K-metasomatism, where values greater than 2 are characteristic of metasomatized rocks and are associated with high K_2O/Na_2O values.

REE concentrations showed almost no change during K-metasomatism; however, some small variations can be observed (Table 2). La, Pr, Sm, Gd and Tb maintain their concentrations, with only a small decrease in their variability. An opposite behavior is observed for Ce, Nd, Dy, Ho, Er, Tm, Yb and Lu which show homogeneous behavior typified by a slight decrease in concentration and almost no change in variability. Finally, Eu concentrations show the highest decrease in concentrations among the REE group. An enrichment/depletion diagram for trace and rare earth elements (Fig. 7) is characterized by enrichment of 68.9% for Rb, of 46.3% for Cs and of 12.5% for Ta. Strong depletion is observed in Sr with a 68.37% loss, and minor depletion factors are seen for Zr (−18.67%), Eu (−20%), and U (−36.96%). Finally Y, Nb, Ba, La, Ce, Pr, Nd, Sm, Gd, Tb, Dy, Ho, Er, Tm, Yb, Hf, Lu, and Th show enrichment/depletion factors between 10 and −10% and are therefore considered as immobile elements (Hollocher et al., 1994).

3.1.3. Metals concentration

Fig. 8 and Table 2 show the behavior of some metals of metallogenic interest during increasing K-metasomatism. As shown previously, the K_2O/Na_2O ratio is used as an alteration intensity index. Precious metals are represented by Au and Ag, and as can be seen in Fig. 8a, Au contents show both an increase in concentration and in variability. The Ag contents are mostly below the detection limit of 0.1 ppm (Fig. 8b) making it difficult to extract information about its behavior during metasomatism. However, the number of assays over the detection limit observed in the altered rocks is higher than in their unaltered equivalents, suggesting an increase in Ag content during metasomatism. Among base metals, Cu is characterized by a small increase in concentration but a decrease in variability (Fig. 8c); whereas Pb and Zn both decreased in their content and variability (Fig. 8d and e). Moreover, As and Sb behaved in a similar way during alteration (Fig. 8f and g), with a slight increase in concentration during metasomatism. However, their variability change is the opposite, with a decrease in As and a increase in Sb as is shown in the dataset. The Hg content shows the same problem as with Ag, with most samples below the detection limit of 0.01 ppm (Fig. 8h). Nonetheless content probably increased during metasomatism based on the number of assays over the detection limit in the K-metasomatized field. Finally, W is characterized both by an increase in content and variability, whereas Mo remains almost constant with a small decrease in variability (Table 2).

The enrichment/depletion diagram for metals (Fig. 9) is characterized by a strong enrichment of about 100% in Au, Sb and W, and also a minor enrichment in Cu (16.25%) and As (8.33%). Elements showing depletion are Pb (−24.63%) and Zn (−41.1%); finally Mo remains unchanged. Ag and Hg variations are obscured due to the number of samples below the instrument detection limit, but even they seem to increase during metasomatism. However, these data should be taken with caution, and as such Ag and Hg were not considered in the construction of Fig. 9.

4. Discussion

K-metasomatism has been recognized in several localities around the world and in different geological settings. However, in most cases the affected rocks are acid volcanics, especially ash flow tuffs of dacitic to rhyolitic composition (Agron and Bentor, 1981; Scherkenbach and Noble, 1984; Brooks, 1988; Cooke et al., 1998; Ennis et al., 2000; Smolak and Michalik, 2002). While K-metasomatism seems to be a common characteristic of extensional environments (Hollocher et al., 1994; Beratan, 1999; Cooke et al., 1998), it also has been described in

Author's personal copy

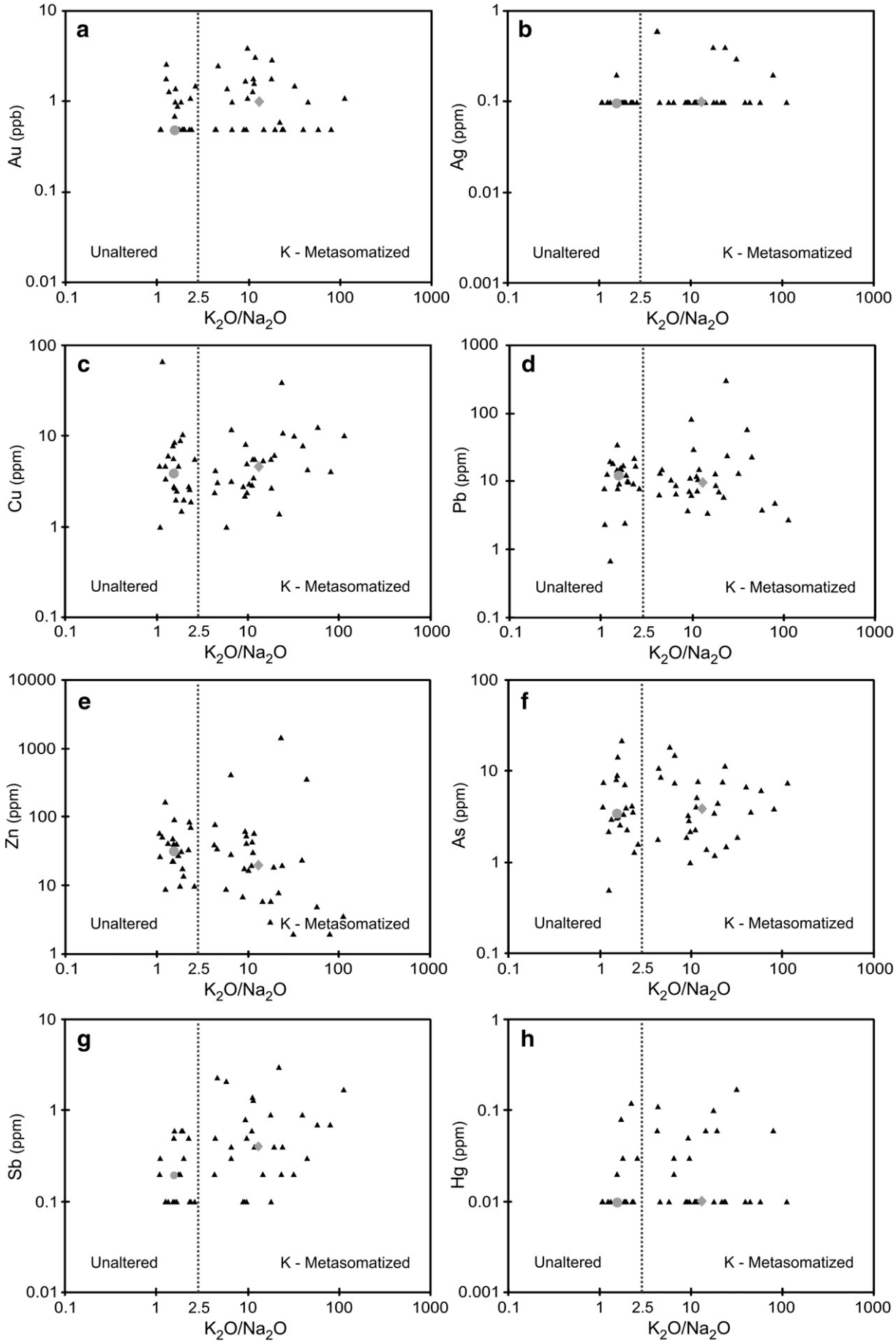

Author's personal copy

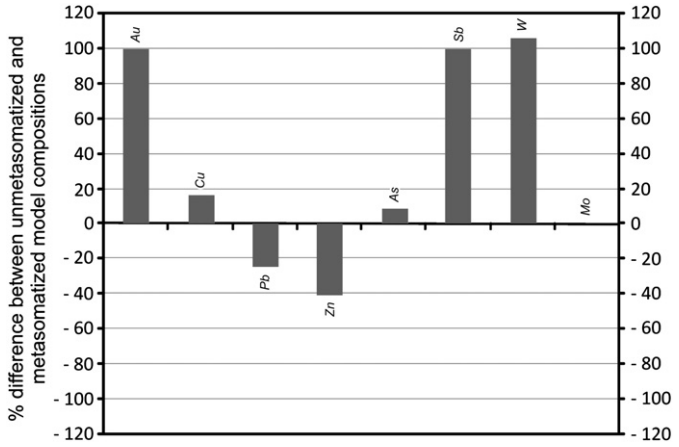

Fig. 9. Enrichment/depletion diagram for metals summarizing the compositional changes occurred during K-metasomatism. The percent compositional change is based on median values of unaltered compared to metasomatized samples, respectively, as expressed in Table 2; positive values indicate enrichment in K-metasomatized rocks, while negative values indicate leaching.

volcanic arc environments (Scherkenbach and Noble, 1984). Metamorphic, hydrothermal and diagenetic fluid origins have been proposed for different altered areas.

Like many K-metasomatized areas, the BLVC was erupted in an extensional setting, and all affected rocks are characterized by silica contents higher than 68 wt.% (dacitic to rhyolitic ash flow tuffs and lavas), leaving the less differentiated members of Jurassic volcanism virtually unaffected. In addition, BLVC metasomatized rocks suffered an intense geochemical change, as can be seen in Figs. 5, 7 and 9. These changes are comparable to those reported for other metasomatized regions of the Western United States (Hollocher et al., 1994; Ennis et al., 2000) and Northern Australia (Cooke et al., 1998), suggesting that K-metasomatic processes have a similar geochemical signature in different localities.

The strong similarities in the lithologies and geochemical signatures implies that volcanic glass could play an important role as an ion exchanger during K-metasomatism, as is supported by experimental and field data from Lofgren (1970), Scott (1970), Kochhar (1977), Shiraki and Iiyama (1990) and Steinhauser and Bichler (2008).

Mineralogical changes occurring during K-metasomatism are very difficult to recognize in hand specimen and in many cases also on thin sections. This is especially true considering the glassy nature of most altered samples. The typical secondary mineral assemblage reported for K-metasomatized areas is composed of adularia + quartz ± hematite ± clay minerals (Ennis et al., 2000; Rougvie and Sorensen, 2002). Mineralogical studies show that K-metasomatism strongly affects Na-rich minerals, especially plagioclases, while K-rich minerals remain almost unchanged (Ennis et al., 2000), except during extreme metasomatism, when K-rich mineral phases (e.g., sanidine) are replaced (Rougvie and Sorensen, 2002).

Mineralogical changes occurring during K-metasomatism on the BLVC rocks were studied on 25 thin sections from known metasomatized areas within the Deseado Massif (Fig. 1). The most dramatic mineralogical change observed is the complete replacement of plagioclase by K-feldspar (variety adularia) even in samples with little metasomatism (low K_2O/Na_2O ratio) (Fig. 10a). Alkali feldspar is also replaced by adularia on moderate to highly altered samples (Fig. 10b), while sanidine and biotite remains almost unaltered even under strong metasomatic conditions. Original groundmass textures like glass shards, eutaxitic textures, flow banding and felsitic textures are likely to be preserved, but completely replaced by adularia or adularia + quartz aggregates (Fig. 10c).

In the Deseado Massif, a low volatile K-metasomatic mineral association is also suggested by the low L.O.I. values observed in the metasomatized rocks. This observation, combined with the incorporation of high amounts of K_2O and Rb, is coherent with the formation of adularia as the new mineral phase during K-metasomatism. The new mineral assemblage strongly replaces plagioclase (Fig. 10a), characterized by losses of Na_2O, CaO, Sr and minor losses in Eu. The 1:1 molar K:Na exchange ratio observed in the BLVC metasomatic trend (Fig. 3) indicates that added K_2O largely replaces the Na_2O present in the albite component of plagioclase and alkali feldspar phenocrysts (Fig. 10a and b), and especially in the glassy matrix (Fig. 10c) as it was also suggested by Hollocher et al. (1994) and Ennis et al. (2000).

Finally, the presence of at least two additional, non-metasomatic alteration types can be recognized using geochemical data from the BLVC (Fig. 2). The immobile behavior of silica during increasing metasomatism (Fig. 4a) indicates that samples with silica values above 78 wt.% (Fig. 2a) correspond to a silicification event not related to K-metasomatism. A second alteration type in the non-metasomatized rocks is characterized by a progressive decrease in the K_2O/Na_2O ratio along with an increase of L.O.I. values (Fig. 2b). This variation indicates the leaching of potassium along with incorporation of volatile components probably due to transformation of feldspars to kaolinite, and is probably related to weathering of the volcanic pile.

4.1. Influence of K-metasomatism in petrologic discrimination diagrams

The effects of K-metasomatism on BLVC whole-rock geochemistry produced significant concentration changes in many elements commonly used for classification and tectonic discrimination in igneous petrology. The most obvious change is developed in the content of alkalis on the metasomatized group of rocks, where the increase of K_2O and decrease in Na_2O is produced with no change in SiO_2. When these changes are analyzed in a TAS diagram (Le Maitre, 1989), the K-metasomatized samples (Fig. 11a) show a strong dispersion along the alkalis axis, with an overall increase compared to the unaltered rocks (Fig. 11b). As the silica content is not so affected by K-metasomatism, both diagrams cover a very similar silica range. The strong enrichment in K_2O also produces a migration of the metasomatized samples towards the Shoshonitic field in the K_2O vs. SiO_2 diagram of Peccerillo and Taylor (1976) (fig. 2, p. 66). On an AFM diagram (Irvine and Baragar, 1971), the losses on FeOt and MgO combined with the increase in the content of alkalis tend to concentrate all K-metasomatized samples toward the alkalis corner of the triangular diagram, also increasing their dispersion.

Due to the high mobility of major elements that occurred during K-metasomatism, no classification or discrimination diagram is considered to be valid for chemical characterization of volcanic rocks based on metasomatized rocks. Instead, Winchester and Floyd (1977) used immobile elements to classify altered volcanic rocks. These diagrams are based on SiO_2, Zr, Nb and Ce, all elements which remain constant during increasing metasomatism. However, some immobile element diagrams also use TiO_2, which suffers much variation during metasomatism. For Deseado Massif samples, the effect of titanium leaching on the Zr/TiO_2 vs. Nb/Y diagram is not evident, and is mostly represented by an increase in sample dispersion. Nonetheless, the use of TiO_2 in immobile element classification schemes must be used with caution because of its strong depletion in metasomatized rocks, and thus is not recommended.

For tectonic discrimination, one of the most widely used is the Pearce et al. (1984) diagram Rb vs. (Y + Nb). However, this element is

Fig. 8. Plots between the K_2O/Na_2O ratio and metals. The grey circles and diamonds represent the median compositions of unaltered and metasomatized samples, respectively, as expressed in Table 2. All plotted samples have SiO_2 contents above 68 wt.%.

Author's personal copy

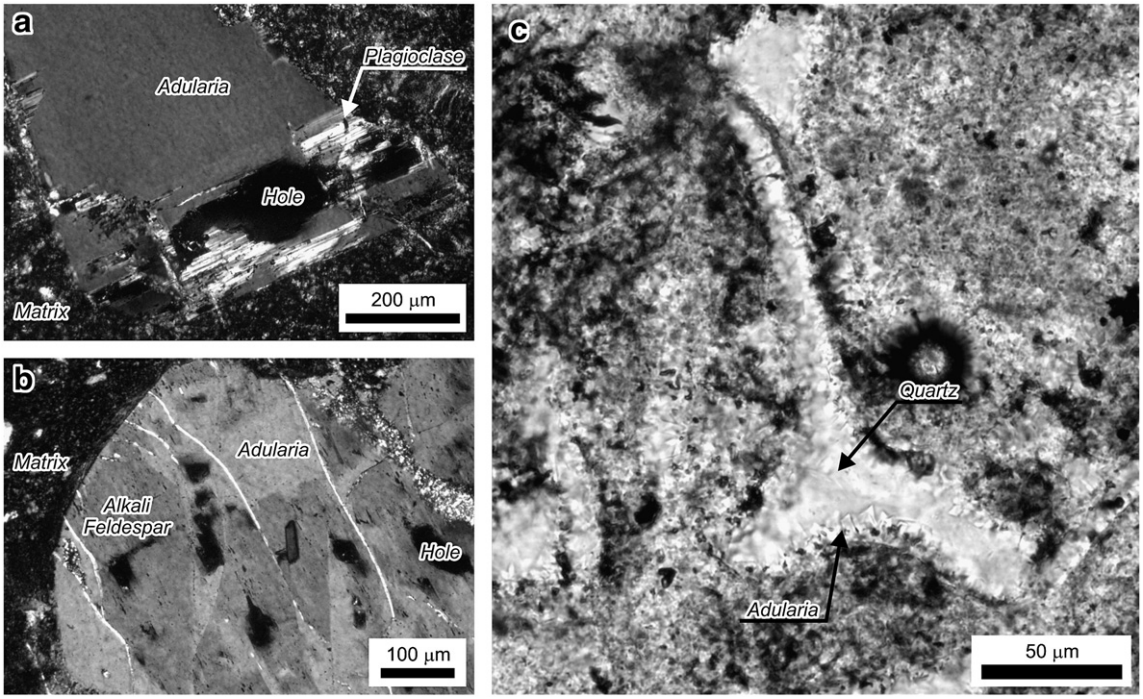

Fig. 10. Mineralogical changes occurring during K-metasomatism on acid rocks from the Deseado Massif; a) Microscopic view under crossed polarizers of a plagioclase crystaloclast from Primero de Abril area showing replacement by adularia (sample M9073, $Na_2O/K_2O = 2.6$); b) Alkali feldspar crystal from Martha Mine area partially replaced by adularia, view under crossed polarizers (sample M6761, $Na_2O/K_2O = 9.68$); c) Microphoto under plain light of a glass shard from Pingüino area showing a complete replacement by adularia and quartz (sample M5731, $Na_2O/K_2O = 112.63$).

also the most affected by the K-metasomatism. The higher Rb content in the altered samples of this study moves almost the entire set of samples from the volcanic arc field (Fig. 11c) to the syn-collisional field (Fig. 11d), potentially leading to misinterpretation of the geotectonic origin of these metasomatized samples. The immobile behavior of most trace elements and REE, with the exception of Rb, Sr, Cs and TiO_2, makes the use of these elements the only trustworthy geochemical tool to evaluate petrological history in metasomatized rocks.

A final comment is made here in reference to geochronological age determinations, particularly in use of the K/Ar, Ar/Ar, and Rb/Sr methods. As strong enrichment in K and Rb, as well as leaching of Sr are observed in metasomatized rocks, with little or no changes in the hand sample level of observation, it is essential that samples are subjected to initial geochemical assessment of the K_2O/Na_2O ratio to avoid those samples which will reflect ages influenced by alteration processes.

4.2. Fluid origin and metallogenic consequences of K-metasomatism

Glassy acid volcanic rocks are very susceptible to post-emplacement modification by devitrification, hydration and hydrothermal alteration, particularly at high temperatures prior to their final cooling, and especially with interaction of alkali-rich solutions (Lofgren, 1970; Scott, 1970; Kochhar, 1977; Shiraki and Iiyama, 1990). Three different sources have been proposed for the K-metasomatizing fluids recognized in several locations around the world: (1) metamorphic, (2) diagenetic, or (3) hydrothermal.

Low-temperature burial metamorphism has been proposed to be responsible for the K-metasomatized rocks of the Deseado Massif (Gust et al., 1985). However, hydrocarbon exploration carried out on the eastern and southern portions of the Deseado Massif shows that BLVC rocks of La Matilde Formation has vitrinite reflectance indexes between 0.83 and 1.12% R_o (Cortiñas et al., 2005), which is indicative of diagenetic burial temperatures between 130° and 160 ° C (Burnham and Sweeney, 1989). The absence of metamorphism younger than mid-Paleozoic in the Deseado Massif (Giacosa et al., 2002; Guido, 2002; Ramos, 2002), and the diagenetic temperatures observed in the BLVC makes difficult to explain the metasomatic rocks by metamorphism of the volcanic pile.

A low-temperature (<150 °C) diagenetic model has been also proposed to explain K-metasomatism; this is the more favored model to explain large altered areas across the Southwestern United States. This particular model invokes the long term circulation of alkali-rich brines derived from saline lakes formed in closed arid basins (Cooke et al., 1998; Beratan, 1999; Ennis et al., 2000; Rougvie and Sorensen, 2002). The absence of playa or evaporitic lacustrine deposits in the Deseado Massif area, in addition to the proposed warm temperate climate with dry summers for the Jurassic (Cravero et al., 1991; Rees et al., 2000; Sellwood and Valdes, 2006), makes difficult to relate the observed K-metasomatism to diagenetic fluids similar to those reported for the Southwestern United States.

Also magmatic or mixed magmatic–meteoric hydrothermal solutions have been proposed to be the responsible of K-metasomatism in several areas (Agron and Bentor, 1981; Scherkenbach and Noble, 1984; Bartley and Glazner, 1985; Hollocher et al. 1994; Mishin, 2006), the close association between metasomatized rocks and hydrothermal manifestations in the Deseado Massif suggest a genetic link between them.

K-metasomatism in the BLVC modified rock metal concentrations, producing a significant addition in Au, Sb, Cu, As and probably some addition of Ag and Hg, accompanied by depletion of Pb and Zn (Figs. 8 and 9). This geochemical association is typical of the higher parts of low sulfidation hydrothermal environments (Sillitoe, 1993; White and Hedenquist, 1995) and these trends are also comparable to the metal anomalies observed in the Deseado Massif epithermal deposits (Schalamuk et al., 1997; Echeveste, 2001; Ruiz and Guido, 2006). The depletion in Pb and Zn is also compatible with the observed low proportion of base metal minerals in the veins and breccias, which are mainly quartz ± adularia rich, with less than 10% metalliferous minerals (Guido and Schalamuk, 2003; Echavarría et al., 2005; Fernandez et al., 2008).

Author's personal copy

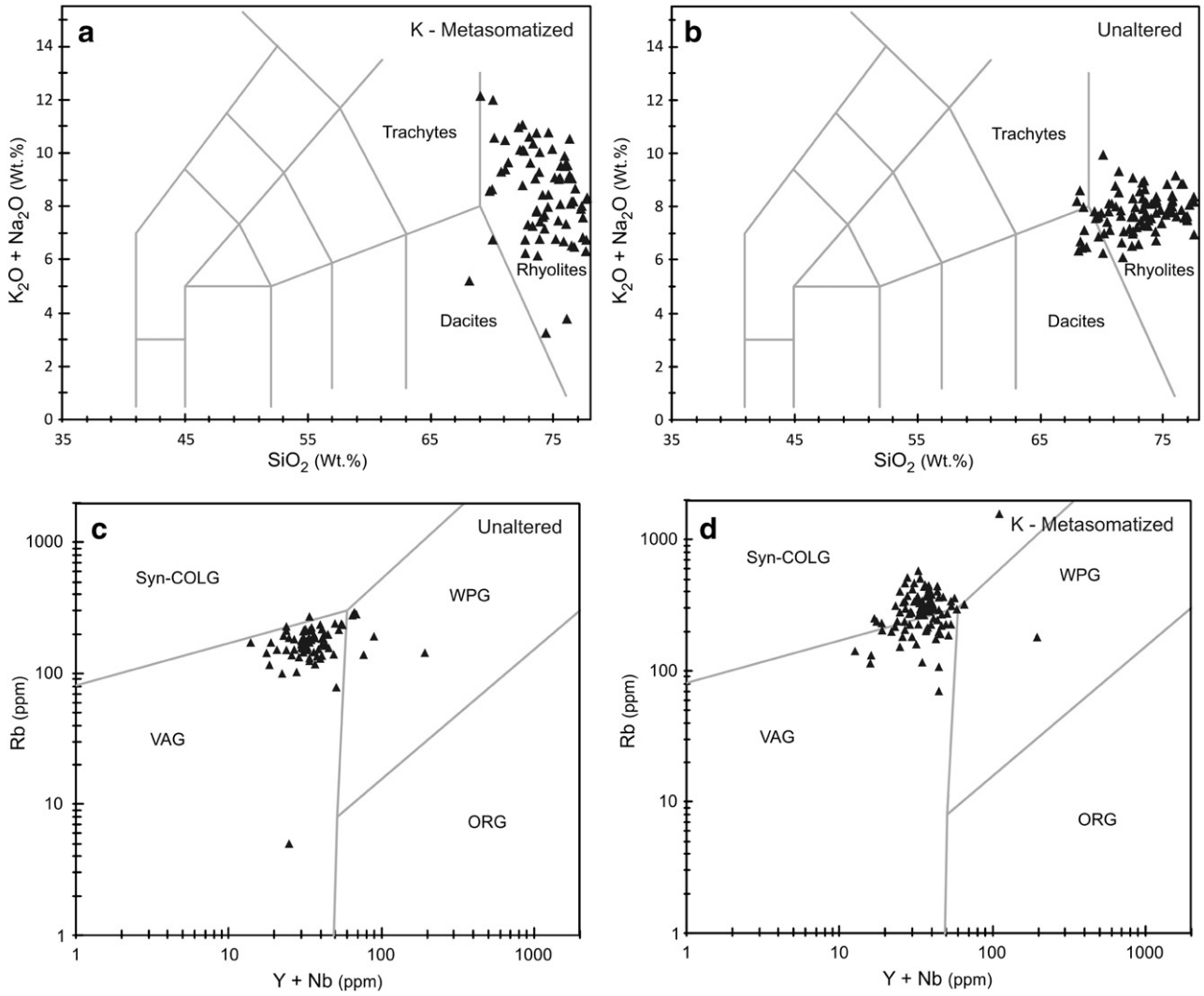

Fig. 11. Influence of K-metasomatism on petrologic diagrams. See text for details.

Unlike the intermediate rocks of the Bajo Pobre Formation, which are mainly composed of small and relatively thin andesitic flow units, the acid volcanics of the Chon Aike Formation build thick ash flow cooling units of more than 100 m, and lava dome complexes of more than 1 km diameter (Guido, 2002; Ruiz et al., 2008; Echeveste, 2001). The thick volcanic deposits of the Chon Aike Formation represent the late eruption products of the BLVC, and probably constitute the heat source of the hydrothermal cells that created most epithermal deposits of the Deseado Massif.

The circulation of hot hydrothermal fluid combined with the high ion exchange capacity of glassy rocks of the Chon Aike Formation is probably the key to explain why K-metasomatism affects only rocks with SiO_2 contents higher than 68%. The Na^+/H^+ and K^+/H^+ ratios of the fluid controls the stability of adularia vs. albite and feldspars vs. clay (Fig. 12). As the studied K-metasomatized areas are developed as distal alteration haloes related to Deseado Massif epithermal systems, an increase in K^+/H^+ is necessary to move from the sericite stability field typical of argillic proximal alteration haloes into the K-feldspar stability field. This can be achieved by an increase of K^+ activity in the solutions, or by a decrease in H^+ activity (an increase in the pH). As the metasomatizing fluids are thought to have an excess of potassium, the most probable factor controlling this transition would have been a decrease in pH, the product of the progressive neutralization of the fluids as they circulated inside the volcanic deposits.

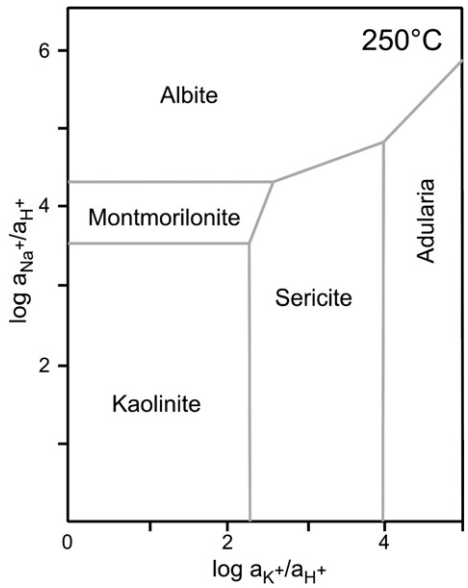

Fig. 12. Activity diagram for the system $Na_2O + K_2O + Al2O_3 + SiO_2 + H_2O$ at 250 ° C.

Author's personal copy

5. Conclusion

K-metasomatism identified in the Bahía Laura Volcanic Complex is difficult to recognize in hand specimen, is characterized by K_2O/Na_2O ratios higher than 2.5 and L.O.I. values lower than 3 wt.%, and affects only rocks with silica contents over 68 wt.%. This metasomatism produced an intense geochemical change in the affected rocks, with the significant addition of K_2O, Rb, Au, Sb, W and a minor enrichment in Cs, Cu, As, and probably Ag and Hg. Strongly depleted elements include MgO, CaO, Na_2O, P_2O_5, MnO, Sr and U whereas FeOt, TiO_2, L.O.I., Pb and Zn are typified by intermediate depletion. Finally, SiO_2, Al_2O_3, Mo, and most trace elements and REE, remained almost invariable during increasing metasomatism.

Strong similarities in lithologies and geochemical signatures observed in K-metasomatized areas around the world, regardless of geological setting and fluid origin, suggests that volcanic glass probably played an important role as an ion exchanger during K-metasomatism. This also explains why only rocks with silica contents higher than 68% are affected in the Deseado Massif BLVC.

Due to the high mobility of elements occurring during K-metasomatism, no classification or discrimination diagram based on major elements, TiO_2 or Rb, are considered to be valid for chemical characterization of volcanic rock samples that have been metasomatized. Instead, trace elements and REE are the more reliable tools for petrologic and petrogenetic interpretations using metasomatized samples.

The precious and base metal enrichment/depletion patterns of K-metasomatized rocks are identical to the geochemical signatures observed in the upper parts of low sulfidation settings in the Deseado Massif. This similarity, along with the spatial relationships observed between K-metasomatized rocks and epithermal manifestations in the field, allows us to propose that hydrothermal fluids were responsible for the metasomatism observed in the Bahia Laura Volcanic Complex. However a deuteric component within the metasomatic fluids cannot be discounted.

Finally, the distal position of the K-metasomatic alteration haloes with respect to the hydrothermal systems, combined with their geochemical signatures, makes this alteration signal an exploration guide for epithermal deposits in the Deseado Massif. In this context, both K_2O/Na_2O and Rb/Sr ratios can be used as good indicators of proximity to epithermal ore deposits.

Acknowledgements

Previously unpublished geochemical assays were performed with the generous support of Coeur d'Alene Mines and Argentex Mining Corporation. We thank Alfredo Cruzat and Ken Hicks for their support. We also appreciate the support, discussions and constructive suggestions given by Kathy Campbell, Martin Muravchik and Luciano Lopez. Finally, we also thank to an anonymous reviewer for valuable comments and suggestions that helped to improve this work.

References

Agron, N., Bentor, Y.K., 1981. The Volcanic Massif of Biq'at Hayareah (Sinai–Negev): a case of potassium metasomatism. J. Geol. 89 (4), 479–495.

Alperin, M., Echeveste, H., Fernandez, R., Giuliano, B., 2007. Análisis estadístico de datos geoquímicos de volcanitas jurásicas del Macizo del Deseado, Provincia de Santa Cruz. Revista de la Asociación Geológica Argentina 62 (2), 200–209.

Arribas Jr, A., Schalamuk, I.B., de Barrio, R., Fernández, R., Itaya, T., 1996. Edades Radimétricas de Mineralizaciones Epitermales Auríferas del Macizo del Deseado, Provincia de Santa Cruz, Argentina. IGCP Project 342: Age and isotopes of South American Ores. XXXIX Congresso Brasileiro de Geología, pp. 254–257.

Bartley, J.M., Glazner, A.F., 1985. Hydrothermal systems and tertiary low-angle normal faulting in the southwestern United States. Geology 13, 562–564.

Beratan, K.K., 1999. Miocene potassium metasomatism, Whipple Mountains, southeastern California: a datable tracer of extension-related fluid transport. Geology 27 (3), 259–262.

Brooks, W.E., 1988. Recognition and geologic implications of potassium metasomatism in upper-plate volcanic rocks at the detachment fault at Harcuvar Mountains, Yavapai County, Arizona. U. S. Geological Survey Open-file Report 88-0017. 9 pp.

Burnham, A.K., Sweeney, J.J., 1989. A chemical kinetic model of vitrinite maturation and reflectance:. Geochimica et Cosmo-chimica Acta 53, 2649–2657.

Busà, T., Bellieni, G., Clocchiatti, R., Echeveste, H., Fernández, R., Piccirillo, E.M., Fantauzzi, G., 2001. Preliminary data on orthopyroxene and quartz-trapped melt inclusions from Patagonia igneous province: evidence on the evolution of magmatic system. GEOITALIA, 3° Forum FIST. Sessione 28, 833–834.

Busà, T., Fantauzzi, G., Bellieni, G., Fernández, R., Echeveste, H., Piccirillo, E.M., 2003. Relationship between Bajo Pobre and Chon Aike Formations (Deseado Massif, Patagonia, Argentina): a melt inclusions study. Geophysical Research Abstracts Vol. 5, 11094.

Cooke, D.R., Bull, S.W., Donovan, S., Rogers, J.R., 1998. K-metasomatism and base metal depletion in volcanic rocks from the McArthur Basin, Northern Territory, implications for base metal mineralization. Economic Geology, Vol. 93, 1237–1263.

Cortiñas, J., Homovc, J., Lucero, M., Gobbo, E., Laffitte, G., Viera, A., 2005. Las cuencas de la región del Deseado, provincia de Santa Cruz. In: Chebli, A.G., Cortiñas, J.S., Spalletti, L.A., Legarreta, L., Vallejo, E.L. (Eds.), Frontera exploratoria de la Argentina. Instituto Argentino del Petróleo y del Gas, pp. 289–305. Buenos Aires.

Cravero, F., Domínguez, E., Murray, H., 1991. Valores δ18O y δD en caolinitas indicadoras de un clima templado húmedo para el Jurásico Superior-Cretácico Inferior de la Patagonia. Revista de la Asociación Geológica Argentina 46 (1–2), 20–25.

de Barrio, R., Panza, J.L., Nullo, F., 1999. Jurásico y Cretácico del Macizo del Deseado, provincia de Santa Cruz. In: Caminos, R. (Ed.), Geología Argentina, anales 29 (17): 511–527. Instituto de Geología y Recursos Minerales.

Echavarría, L. E., 1997. Estudio geológico-minero del área El Dorado-Montserrat, Departamento Magallanes, provincial de Santa Cruz. Universidad Nacional de La Plata. Unpublished PhD Thesis.

Echavarría, L.E., Schalamuk, I.B.A., Etcheverry, R.O., 2005. Geologic and tectonic setting of Deseado Massif epithermal deposits, Argentina, based on El Dorado–Monserrat. Journal of South American Earth Sciences 19, 415–432.

Echeveste, H., 2005. Metalogénesis del distrito argetoaurífero Manantial Espejo, Macizo del Deseado. Provincia de Santa Cruz. Universidad Nacional de La Plata. Unpublished PhD Thesis.

Echeveste, H., Fernandez, R., Bellieni, G., Tessone, M., Llambias, E., Schalamuk, I., Piccirillo, E., Demin, A., 2001. Relaciones entre las Formaciones Bajo Pobre y Chon Aike (Jurásico medio a superior) en el área de Estancia El Fénix–Cerro Huemul, zona centro-occidental del Macizo del Deseado, provincia de Santa Cruz. Revista de la Asociación Geológica Argentina 56 (4), 548–558.

Ennis, D.J., Dunbar, N.W., Campbell, A.R., Chapin, C.E., 2000. The effects of K-metasomatism on the mineralogy and geochemistry of silicic ignimbrites near Socorro, New Mexico. Chemical Geology 167 (3–4), 285–312.

Fantauzzi, G., 2003. Magmatismo Giurassico del Macizo del Deseado (Agentina): studio petrológico e sue implicazioni geodinamiche. Dottorato di Ricerca in "Geofísica della litosfera e geodinamica" XIV ciclo. Universita' Degli Studi di Triesti.

Féraud, G., Alric, B., Fornari, M., Bertrand, H., Haller, M., 1999. $^{40}Ar/^{39}Ar$ dating of the Jurassic volcanic province of Patagonia: migrating magmatism related to Gondwana break-up and subduction. Earth and Planetary Science Letter 172, 83–96.

Fernandez, R.R., Blesa, A., Moreira, P., Echeveste, H., Mykietiuk, K., Andrada de Palomera, P., Tessone, M., 2008. Los depósitos de oro y plata vinculados al magmatismo jurásico de la Patagonia: revisión y perspectivas para la exploración. Revista de la Asociación Geológica Argentina 63 (4), 665–681.

Feruglio, E., 1949. Descripción geológica de la Patagonia. 3 Volumes, Dirección Nacional de Yacimientos Petrolíferos Fiscales, Buenos Aires.

Giacosa, R., Marquez, M., Panza, J., 2002. Basamento Paleozoico inferior del Macizo del Deseado. In: Haller, M. (Ed.), Geología y Recursos Naturales de la provincia de Santa Cruz. Relatorio del XV Congreso Geológico Argentino, El Calafate, I-2, pp. 33–44.

Gonzalez Guillot, M., De Barrio, R., Ganem, F., 2004. Mina Martha, un Yacimiento Epitermal Argentifero en el Macizo del Deseado, Provincia de Santa Cruz. VII Congreso de Mineralogía y Metalogenia, Actas 119–204 Río Cuarto.

Guido, D., 2002. Geología y metalogénesis del sector oriental del Macizo del Deseado, provincia de Santa Cruz. Universidad Nacional de La Plata. Unpublished PhD Thesis.

Guido, D., 2004. Subdivisión litofacial e interpretación del volcanismo jurásico (Grupo Bahía Laura) en el este del Macizo del Deseado, provincia de Santa Cruz. Revista de la Asociación Geológica Argentina 59 (4), 727–742.

Guido, D., Schalamuk, I., 2003. Genesis and exploration potential of epithermal deposits from the Deseado Massif, Argentinean Patagonia. In: Eliopoulos, et al. (Ed.), Mineral Exploration and Sustainable Development. Balkema–Rotterdam, Vol I, pp. 493–496.

Guido, D.M., Jovic, S.M., Schalamuk, I.B., 2005. A new metallogenic association (Sn–Cd–In–Zn–Ag–Au) in the Deseado Auroargentiferous province, Deseado Massif, Patagonia, Argentina. Mineral Deposit Research: Meeting the Global Challenge—8th SGA Meeting, Beijing, China, Volume 2, pp. 965–968.

Guido, D., Escayola, M., De Barrio, R., Schalamuk, I., Franz, G., 2006. La Formación Bajo Pobre (Jurásico) en el este del Macizo del Deseado, Patagonia Argentina: Vinculación con el Grupo Bahía Laura. Revista de la Asociación Geológica Argentina 61 (2), 187–196.

Gust, D.A., Biddle, K.T., Phelps, D.W., Uliana, M.A., 1985. Associated middle to late Jurassic volcanism and extension in southern South America. Tectonophysics 116, 223–253.

Hollocher, K., Spencer, J., Ruiz, J., 1994. Composition changes in ash-flow cooling unit during K-metasomatism, West-Central Arizona. Economic Geology, Vol. 89, 877–888.

Irvine, T., Baragar, W., 1971. A guide to the chemical classifications of the common volcanics rocks. Canadian Journal of Earth Science 8, 523–548.

Author's personal copy

Jovic, S.M., 2009. Geología y metalogénesis de las mineralizaciones polimetálicas del área El Tranquilo (Cerro León), Sector Central del Macizo del Deseado, Provincia de Santa Cruz. Universidad Nacional de La Plata. Unpublished PhD Thesis.

Jovic, S.M., Jovic, N., Guido, D.M., Schalamuk, I.B., 2008. Caracterización de cuerpos intrusivos de la formación Cerro León en el área del Anticlinal el Tranquilo, Macizo del Deseado, Santa Cruz. XVII Congreso Geológico Argentino. Actas (II), pp. 851–852. Jujuy, Argentina.

Kochhar, N., 1977. Post-emplacement alkali modifications in rapidly cooled acid volcanic rocks. American Mineralogist, Volume 62, 333–335.

Le Maitre, R.W., 1989. A Classification of Igneous Rocks and Glossary of Terms. Blackwell, Oxford. 193 pp.

Lofgren, G., 1970. Experimental devitrification rate of rhyolite glass. Geological Society of America Bulletin 81, 553–560.

López, R., 2006. Estudio Geológico-Metalogenético del area oriental al curso medio del Río Pinturas, sector noroeste del Macizo del Deseado, provincia de Santa Cruz, Argentina. Universidad Nacional de La Plata. Unpublished PhD Thesis.

Mishin, L.F., 2006. The nature and prospecting implications for ultrapotassic rhyolites as exemplified by epithermal gold–silver deposits of the Far East. Pacific Geology Vol. 25 (6), 30–39 In Russian.

Moreira, P., 2005. Geología y Metalogénesis del Distrito La Josefina, Macizo del Deseado, Provincia de Santa Cruz. Universidad Nacional de La Plata. Unpublished PhD Thesis.

Pankhurst, R.S., Rapela, C.W., 1995. Production of Jurassic rhyolite by anatexis of the lower crust of Patagonia. Earth and planetary Science Letters 134, 23–36.

Pankhurst, R., Leat, P., Sruoga, P., Rapela, C., Marquez, M., Storey, B., Riley, T., 1998. The Chon Aike province of Patagonia and related rocks in West Antartica: a silicic large igneous province. Journal of Volcanology and Geothermal Research 81, 113–136.

Pankhurst, R., Riley, T., Fanning, C., Kelley, S., 2000. Episodic Silicic Volcanism in Patagonia and the Antarctic Peninsula: chronology of magmatism associated with the Break-up of Gondwana. Journal of Petrology 41, 605–625.

Panza, J.L., Haller, M.J., 2002. El volcanismo jurásico. In: Haller, M.J. (Ed.), Geología y recursos Naturales de Santa Cruz. Relatorio del XV Congreso Geológico Argentino, pp. 89–102.

Pearce, J.C., Harris, N.B.W., Tindle, A.G., 1984. Trace element discrimination diagrams for the tectonic interpretation of granitic rocks. Journal of Petrology 25 (4), 956–983.

Peccerillo, R., Taylor, S.R., 1976. Geochemistry of Eocene calc-alkaline from the Kastamonu area, Northern Turkey. Contributions to Mineralogy and Petrology (58), 63–81.

Permuy, C., Guido, D., 2008. Centro volcánico mineralizado de Estancia La Invernada, Macizo del Deseado, Provincia de Santa Cruz. XVII Congreso Geológico Argentino. Actas (III), pp. 1451–1452. Jujuy, Argentina.

Ramos, V., 2002. Evolución Tectónica. In: Haller, M. (Ed.), Geología y Recursos Naturales de Santa Cruz. Relatorio del XV Congreso Geológico Argentino. El Calafate, I–23, pp. 235–387.

Rees, P.M., Ziegler, A.M., Valdes, P.J., 2000. Jurassic phytogeography and climates: new data and model comparisons. In: Huber, B.T., Macleod, K.G., Wing, S.L. (Eds.), Warm Climates in Earth History. Cambridge Univ. Press, pp. 297–318.

Riley, T., Leat, P., Pankhurst, R., Harris, C., 2000. Origin of large volume rhyolitic volcanism in Antartic Peninsula and Patagonia by crustal melting. No. 6 Journal of Petrology 42, 1043–1065.

Rougvie, J.R., Sorensen, S.S., 2002. Cathodoluminescence record of K-metasomatism in ash-flow tuffs: grain-scale mechanisms and large-scale geochemical implications. Geology 30 (4), 307–310.

Ruiz, R., Guido, D.M., 2006. Metal geochemistry from epithermal deposits of the Deseado Massif, Patagonia, Argentina. First International SEG Student Chapter Conference—SEG 2006, Biennial Conference "Wealth Creation in the Minerals Industry", Abstracts, pp. 354–355. Colorado, USA.

Ruiz, R., Paez, G.N., Guido, D.M., Schalamuk, I.B., 2008. Ambiente volcánico y mineralizaciones del Área Cerro 1ro de Abril, Sector Sudoccidental del Macizo del Deseado, Santa Cruz, Argentina. XVII Congreso Geológico Argentino. Actas (II), pp. 897–898. Jujuy, Argentina.

Schalamuk, I., Zubia, M., Genini, A., Fernández, R., 1997. Jurassic epithermal Au–Ag deposits of Patagonia, Argentina. Ore Geology Reviews 12 (3), 173–186.

Schalamuk, I., de Barrio, R., Zubia, M., Genini, A., Echeveste, H., 1999. Provincia Auroargentífera del Deseado, Santa Cruz. In: Recursos Minerales de la República Argentina (Ed. E. Zappettini), Instituto de Geología y Recursos Minerales SEGEMAR. Anales 35, 1177–1188.

Schalamuk, I.B., Ríos, F.J., de Barrio, R.E., Moreira, P., Fuzikawa, K., Echeveste, H., Cunningham, C., Vieira Alves, J., 2005. Mineralized fluids related to Au–Ag ores in selected districts of epithermal province Macizo del Deseado, Southern Patagonia, Argentina. XVI Congreso Geológico Argentino, Actas, 2, pp. 355–360. La Plata, Argentina.

Scherkenbach, D.A., Donald, C., Noble, D.C., 1984. Potassium and rubidium metasomatism at the Julcani District, Peru. Economic Geology Vol. 79 (3), 565–572.

Scott, R.B., 1970. Alkali exchange during devitrification and hydration of glasses in ignimbrite cooling units. The Journal of Geology 79 (1), 100–110.

Sellwood, B.W., Valdes, P.J., 2006. Mesozoic climates: general circulation models and the rock record. Sedimentary Geology 190, 269–287.

Shiraki, R., Iiyama, J.T., 1990. Na–K ion exchange reaction between rhyolitic glass and (Na, K)Cl aqueous solution under hydrothermal conditions. Geochimica et Cosmochimica Acta, Volume 54 (11), 2923–2931.

Sillitoe, R.H., 1993. Epithermal models: genetic types, geometrical controls and shallow features, in Mineral Deposit Modelling (Eds: R V Kirkham et al). Geol Assoc Canada, Spec Pap 40, 403–418.

Smolak, W., Michalik, M., 2002. The Lower Permian Filipowice Tuff — are there primary components in it?. Mineralogical Society of Poland 20, 201–204 Special Papers.

Sruoga, P., 1989. Estudio petrológico del Plateau ignimbrítico jurásico a los 47°30′ de latitud sur. Universidad Nacional de La Plata. Unpublished PhD Thesis.

Steinhauser, G., Bichler, M., 2008. Adsorption of ions onto high silica volcanic glass. Applied Radiation and Isotopes 66 (1), 1–8.

White, N.C., Hedenquist, J.W., 1995. Epithermal gold deposits: styles, characteristics and exploration No. 23 Society of Economic Geologists Newsletter 1, 9–13.

Winchester, J.A., Floyd, P.A., 1977. Geochemical discrimination of different magma series and their differentiation products using immobile elements. Chemical Geology 20, 325–343.